

Numerical simulation of chorus-driving acceleration of relativistic electrons at extremely low L-shell during geomagnetic storms

Zhen-Xia Zhang(张振霞), Ruo-Xian Zhou(周若贤), Man Hua(花漫), Xin-Qiao Li(李新乔), Bin-Bin Ni(倪彬彬), and Ju-Tao Yang(杨巨涛)

Citation: Chin. Phys. B, 2021, 30 (**10**): 109401. DOI: 10.1088/1674-1056/abf556
Journal homepage: http://cpb.iphy.ac.cn; http://iopscience.iop.org/cpb

What follows is a list of articles you may be interested in

North west cape-induced electron precipitation and theoretical simulation

Zhen-xia Zhang(张振霞), Xin-qiao Li(李新乔), Chen-Yu Wang(王辰宇), Lun-Jin Chen
Chin. Phys. B, 2016, 25 (**11**): 119401. DOI: 10.1088/1674-1056/25/11/119401

A 0.33-THz second-harmonic frequency-tunable gyrotron

Zheng-Di Li(李铮迪), Chao-Hai Du(杜朝海), Xiang-Bo Qi(戚向波), Li Luo(罗里), Pu-Kun Liu(刘濮鲲)
Chin. Phys. B, 2016, 25 (**2**): 029401. DOI: 10.1088/1674-1056/25/2/029401

Study of typical space wave-particle coupling eventspossibly related with seismic activity

Zhang Zhen-Xia, Wang Chen-Yu, Shen Xu-Hui, Li Xin-Qiao, Wu Shu-Gui
Chin. Phys. B, 2014, 23 (**10**): 109401. DOI: 10.1088/1674-1056/23/10/109401

Test particle simulations of resonant interactions between energetic electrons and discrete, multi-frequency artificial whistler waves in the plasmasphere

Chang Shan-Shan, Ni Bin-Bin, Zhao Zheng-Yu, Gu Xu-Dong, Zhou Chen
Chin. Phys. B, 2014, 23 (**8**): 089401. DOI: 10.1088/1674-1056/23/8/089401

Numerical simulation of chorus-driving acceleration of relativistic electrons at extremely low L-shell during geomagnetic storms*

Zhen-Xia Zhang(张振霞)[1,†], Ruo-Xian Zhou(周若贤)[2], Man Hua(花漫)[2], Xin-Qiao Li(李新乔)[3)], Bin-Bin Ni(倪彬彬)[2], and Ju-Tao Yang(杨巨涛)[4]

[1] National Institute of Natural Hazards, MEMC, Beijing 100085, China
[2] Department of Space Physics, School of Electronic Information, Wuhan University, Wuhan 430072, China
[3] Institute of High Energy Physics, Chinese Academy of Sciences, Beijing 100049, China
[4] National Key Laboratory of Electromagnetic Environment, China Research Institute of Radiowave Propagation, Qingdao 266107, China

(Received 5 January 2021; revised manuscript received 28 March 2021; accepted manuscript online 7 April 2021)

During 2018 major geomagnetic storm, relativistic electron enhancements in extremely low L-shell regions (reaching $L \sim 3$) have been reported based on observations of ZH-1 and Van Allen probes satellites, and the storm is highly likely to be accelerated by strong whistler-mode waves occurring near very low L-shell regions where the plasmapause was suppressed. It is very interesting to observe the intense chorus-accelerated electrons locating in such low L-shells and filling into the slot region. In this paper, we further perform numerical simulation by solving the two-dimensional Fokker–Planck equation based on the bounce-averaged diffusion rates. Numerical results demonstrate the evolution processes of the chorus-driven electron flux and confirm the flux enhancement in low pitch angle ranges (20°–50°) after the wave-particle interaction for tens of hours. The simulation result is consistent with the observation of potential butterfly pitch angle distributions of relativistic electrons from both ZH-1 and Van Allen probes.

Keywords: chorus acceleration, extremely low L-shell, numerical simulation, ZH-1 satellite, Van Allen probes

PACS: 94.20.wj, 94.30.Xy **DOI:** 10.1088/1674-1056/abf556

1. Introduction

The Earth's radiation belts consist of inner and outer radiation belts separated by a region known as the slot region with electron flux minimum at around $L \sim 3$. The slot region is thought to be formed by a balance between inward radial diffusion and loss of electrons due to interaction with plasmaspheric hiss.[1–3] It has been discovered that the electron enhancements in the radiation belts are associated with occurrence of geomagnetic storms,[4–6] sometimes the slot region filling events are observed.[7]

Whistler-mode waves are often observed during geomagnetic storms[8–12,17] and are possibly excited by the energetic electron injections. Among them, chorus waves are mostly observed outside the plasmasphere near the equator.[13–16] Magnetospheric chorus waves are thought to be able to play a significant role in rapidly accelerating relativistic radiation-belt electrons.[17–21] Numerical models have demonstrated that relativistic electron flux will reach a maximum level within 15 h after interaction with chorus waves during the recovery phase of storm.[22,23] The chorus-induced loss or acceleration have also been studied by many other space physicists.[24–26] However, most of the past numerical simulations were focused on the outer radiation belt at $L > 4$. In this work, what we are interested in is the simulation of chorus acceleration at extremely low L-shell ($L \sim 3$), which has not yet been studied before.

We have reported that the electrons are accelerated by chorus waves in the extremely low L-shell region during the storm of August 2018 ($L \sim 3$).[27] This event is very meaningful and helpful for us to deeply understand the electron acceleration process in radiation belt physics. Here, in this work, we perform numerical simulation of this event by solving two-dimensional Fokker–Planck equation based on the bounce-averaged diffusion rates at around $L = 3$, present the evolution process of the chorus-driven electron fluxes, and compare the numerical results with the observations from satellites.

2. Observations of chorus acceleration of relativistic electrons in extremely low L-shell

The sun-synchronous ZH-1 satellite[28] was launched in February 2018, with the inclination of 97° flying at an altitude of 507 km. The onboard high energy particle package instruments consist of the low-energy detector (HEPP-L) and the high-energy detector (HEPP-H).[29] HEPP-L can measure the electron fluxes with the energy range from 0.1 MeV to 3 MeV and the proton fluxes with the energy range 2–20 MeV. The energy ranges are divided into 256 energy channels with energy

*Project supported by the National Natural Science Foundation of China (Grant Nos. 41904149 and 12173038), Stable-Support Scientific Project of China Research Institute of Radiowave Propagation (Grant No. A132001W07), and the National Institute of Natural Hazards, Ministry of Emergency Management of China (Grant No. 2021-JBKY-11).

†Corresponding author. E-mail: zxzhang2018@163.com

© 2021 Chinese Physical Society and IOP Publishing Ltd

resolution of $\leq 8.9\%$ at 1 MeV for electron.

The Van Allen probes was operated in near-equatorial orbits with a perigee of $\sim 1.1R_{\rm E}$ and an apogee of $\sim 5.9R_{\rm E}$.[30] By the measurement of magnetic electron ion spectrometer (MagEIS) instrument and relativistic electron-proton telescope (REPT)[31] of energetic particle, composition, and thermal plasma (ECT) suite, we investigate fluxes and pitch angle distributions of MeV electrons in radiation belts and slot region.

The electric and magnetic field instrument suite and integrated science (EMFISIS) instrument provides measurements of electric and magnetic fields of waves.[32] The waveform rceiver (WFR) on the EMFISIS instrument measures wave power spectral density from about 10 Hz to 12 kHz and also provides wave polarization properties including wave normal angle and ellipticity, calculated by the singular value decomposition method.[14]

In Ref. [27] we have analyzed precisely the observation data from the waveform receiver (WFR), the high frequency receiver (HFR) and the relativistic electron-proton telescope (REPT) of Van Allen probes. In this paper we briefly review the main contents about this topic. During the period of 25 August to 1 September 2018, a major geomagnetic storm occurred with the minimum $D_{\rm st} \approx -174$ nT at around 06:00 UT on 26 August, as shown in Fig. 1.

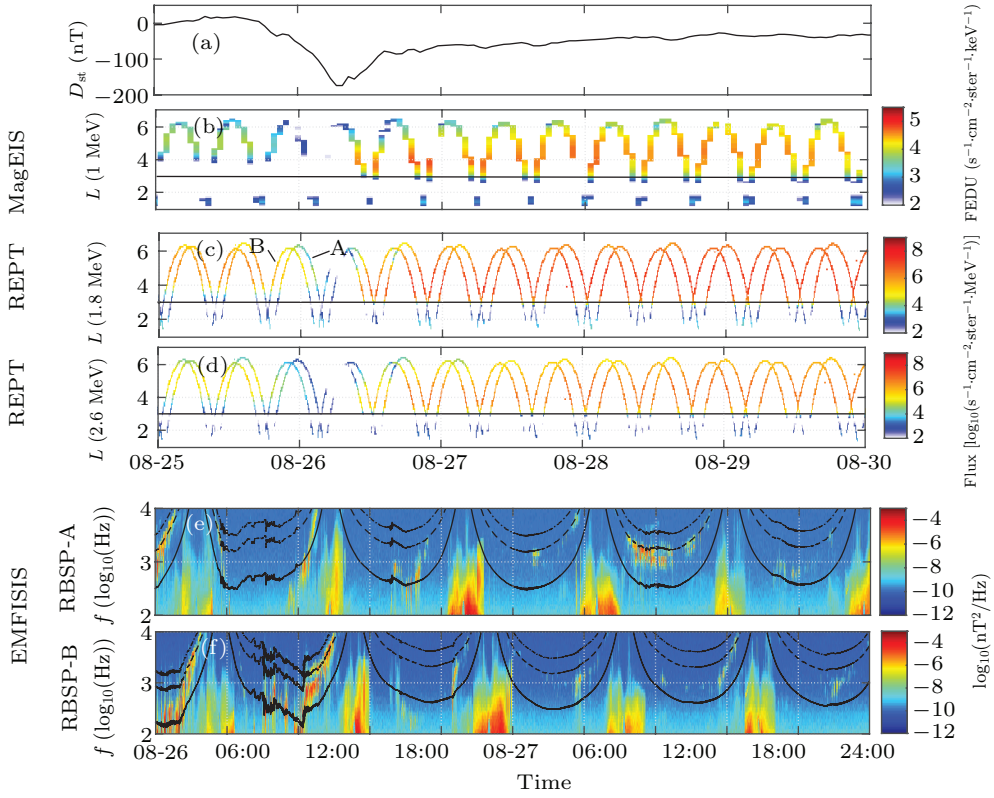


Fig. 1. Overview of the electron evolution during storm of August 2018 observed by Van Allen probes. (a) Geomagnetic storm index $D_{\rm st}$. [(b), (c), (d)] The electron evolution in L-shell for the energy range of 1.0, 1.8 and 2.6 MeV, respectively. [(e), (f)] The electromagnetic signals exited during storms. The solid black lines in panels (b), (c), (d) denote $L = 3$. The black lines in panels (e) and (f) denote $0.1f_{\rm ce}$ (solid), $0.5f_{\rm ce}$ (dashed), and $f_{\rm ce}$ (dotted).

First of all, electron fluxes (1.0, 1.8 and 2.6 MeV) dropped rapidly by a factor of 1–2 orders during the main phase in the duration of 20:00 UT on 25 August to 08:00 UT on 26 August. It is thought that this phenomenon is possibly due to the competition between the acceleration and the loss induced by waves or the $D_{\rm st}$ effect[33,34] or the magnetopause shadowing (because of inward motion of the magnetopause). The flux then gradually increased by 1–2 orders compared to the prestorm level at $L = 3$–6. The flux rose up to the peak value of $\sim 10^7$ $\rm cm^{-2}{\cdot}s^{-1}{\cdot}sr^{-1}{\cdot}keV^{-1}$ in more than 10 h.

Simultaneously, the strong chorus waves were observed obviously on 26 and 27 August as shown in Figs. 1(e) and 1(f), near the appearance moment of the minimum $D_{\rm st}$ index, with frequency 0.1–0.6$f_{\rm ce}$ ($f_{\rm ce}$ is electron gyrofrequency). Figure 2 presents the chorus wave event observed by Van Allen probe B on 26 August 2018, with the strong magnetic spectral density higher than 10^{-4} $\rm nT^2$/Hz in Figs. 2(a)–2(e), reaching up to extremely low L-shells ($L \sim 3$). The wave normal angle is lower than 30°, approximately parallel to the ambient magnetic field (Fig. 2(d)). The ellipticity of these electromagnetic waves is nearly 1, suggesting that the waves are indeed chorus waves with the right-hand polarization mode.

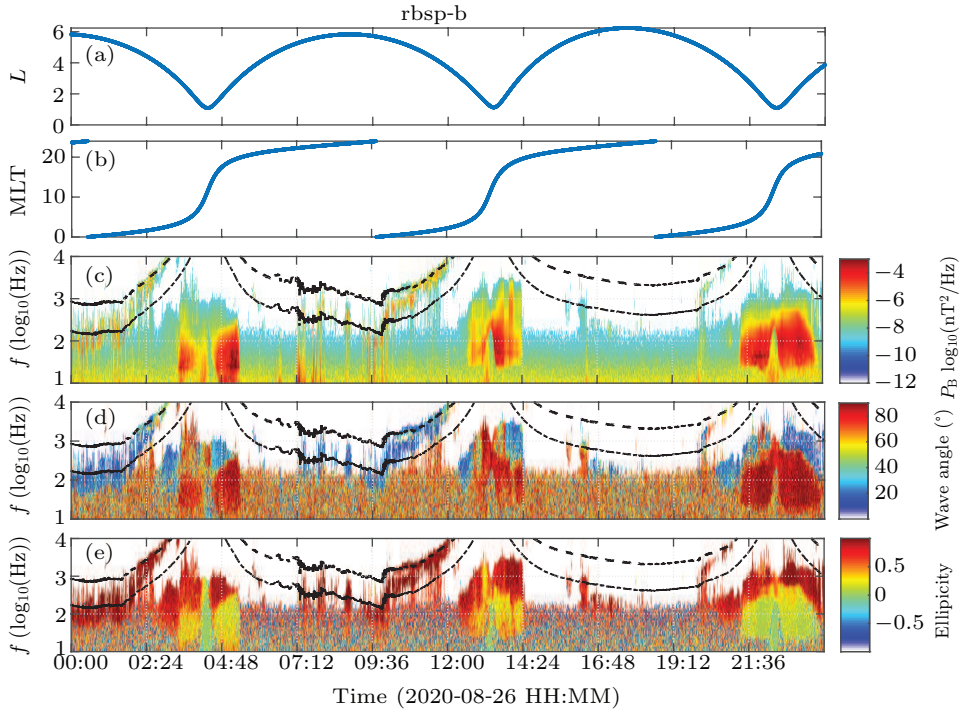


Fig. 2. Waves observed by Van Allen probes B. (a) L-shells, (b) MLT, (c) magnetic field wave spectrum, (d) wave normal angle, (e) ellipticity. The black lines denote electron gyrofrequencies $0.5f_{ce}$ (dashed) and $0.1f_{ce}$ (dotted).

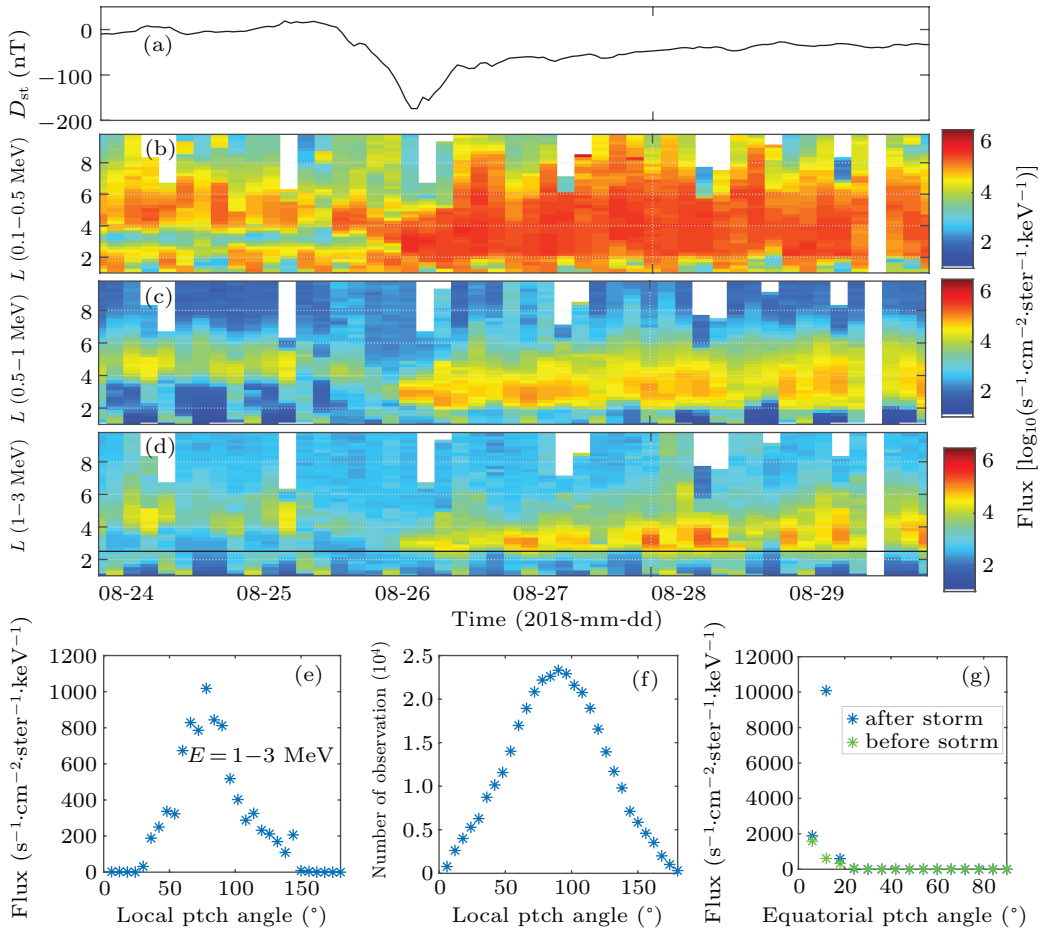


Fig. 3. Overview of the electron evolution during storm of August 2018 measured by ZH-1. (a) The geomagnetic storm index D_{st}. [(b), (c), (d)] The electron evolution for the energy range of 0.1–0.5 MeV, 0.5–1 MeV and 1–3 MeV, respectively. The flux is color coded in logarithm, and sorted in L (L bin: 0.1). [(e), (g)] The flux distributions of 1–3 MeV electrons in local pitch angle and equatorial pitch angle with $L = 2$–5 on August 26 and 27. The data with green stars before storm is taken on August 23 and 24. (f) The number of observed electrons in each pitch angle channel. The solid black line in (d) denotes $L = 3$.

What's more, by the magnetic ephemeris data services in TS04 magnetic field model, using $K = 0.1R_{\rm E}G^{1/2}$ ($R_{\rm E}$ is Earth's radius) and $\mu = 1700$ MeV/G, the phase space density profiles of REPT electrons (1–4 MeV) on August 26 are obtained (see Fig. 5 of Zhang2020 paper). The PSD level increased from $L^* = 2.9$ and formed a peak in $L^* = 2.9$–4 (corresponding to $L = 3.1$–5). The appearance time of the PSD profile growing peaks are consistent with the time of chorus wave observations. This provides a solid evidence for the existence of nonadiabatic process.

The relativistic electron (0.5–3 MeV) flux enhancement at low L-shell is also observed by the ZH-1 satellite (Fig. 3). Particularly, the 1 MeV electron flux is enhanced by about 1–2 orders of magnitude at $L \approx 3$ shown in Figs. 3(b), 3(c), 3(d), which is in agreement with the detection of Van Allen probes. The ZH-1 satellite has an advantage of measuring the electron population with small equatorial pitch angles at the conjugate low altitudes. The transformed equatorial pitch angles in the dipole geomagnetic field are distributed in $< 30^\circ$ shown in Fig. 3(j), which is mainly determined by the satellite observation limitation with respect to the orbit characteristics. Therefore, it is concluded that at least the chorus can play a significant role in accelerating the relativistic electrons efficiently at the small equatorial pitch angles. Also, the butterfly pitch angle distribution of electrons observed by MagEIS and REPT detectors onboard Van Allen probes further verifies this viewpoint (Fig. 6).

The above observation and analysis support that the chorus acceleration tends to play a dominant role in the relativistic electron enhancements even in low L-shell (at least low to $L \sim 3$). In the next section, we present the numerical simulation process and show the results.

3. Numerical simulation of chorus acceleration of relativistic electrons

3.1. Formula of the two-dimensional Fokker–Planck equation

The quasi-linear diffusion equation has been developed as a practical and convenient form of wave-particle interaction theory in radiation belts. Simply in the dipole field situation, based on the diffusion equation including both pitch angle and momentum diffusion terms, the Fokker–Planck equation can be written as

$$\frac{\partial f}{\partial t} = \frac{1}{Gp}\frac{\partial}{\partial \alpha_e}\left[G\left(\langle D_{\alpha\alpha}\rangle \frac{1}{p}\frac{\partial f}{\partial \alpha_e} + \langle D_{\alpha p}\rangle \frac{\partial f}{\partial p}\right)\right] + \frac{1}{G}\frac{\partial}{\partial p}\left[G\left(\langle D_{p\alpha}\rangle \frac{1}{p}\frac{\partial f}{\partial \alpha_e} + \langle D_{pp}\rangle \frac{\partial f}{\partial p}\right)\right]. \quad (1)$$

Based on the hybrid finite difference (HFD) method,[22] we solve the 2-D bounce-averaged Fokker–Planck equation (1), where f is the electron phase space density (PSD), p is the electron momentum, $G = p^2 T(\alpha_{\rm E}) \sin\alpha_e \cos\alpha_e$, with α_e being the equatorial pitch angle.

The $\langle D_{\alpha\alpha}\rangle$, $\langle D_{pp}\rangle$, and $\langle D_{p\alpha}\rangle$ terms correspond to the bounce-averaged diffusion coefficients for the pitch angle diffusion, momentum diffusion, and their mixed term, respectively, specifically having the following formula:

$$\langle D_{\alpha\alpha}\rangle = \frac{1}{T}\int_0^{\lambda_{\rm m}} {\rm d}\lambda D_{\alpha\alpha}\frac{\cos\alpha}{\cos^2\alpha_{\rm e}}\cos^7\lambda, \quad (2)$$

$$\langle D_{\alpha p}\rangle = \frac{1}{T}\int_0^{\lambda_{\rm m}} {\rm d}\lambda D_{\alpha p}\frac{(1+3\sin^2\lambda)^{1/4}}{\cos\alpha_{\rm e}}\cos^4\lambda, \quad (3)$$

$$\langle D_{pp}\rangle = \frac{1}{T}\int_0^{\lambda_{\rm m}} {\rm d}\lambda D_{pp}\frac{(1+3\sin^2\lambda)^{1/2}}{\cos\alpha}\cos\lambda, \quad (4)$$

where $\lambda_{\rm m}$ denotes the latitude of the bounced-particle mirror point.

The wave-frequency spectrum density is assumed to obey a Gaussion distribution, which is modeled by observed chorus wave from detection of Van Allen probes during the recovery phase of the storm. Thus, we adopt the fitted parameters of chorus wave with amplitude $B_{\rm w} = 88$ pT, central frequency $f_{\rm m} = 0.19 f_{\rm ce}$ ($f_{\rm ce}$ is electron gyrofrequency), width 0.057 $f_{\rm ce}$ at $L = 3.5$. The $f_{\rm ce}$ value is 45.7 kHz at $L = 3$. The detailed parameters of waves are shown in Figs. 4(j) and 4(k). With the field-aligned electromagnetic wave, the closed analytical form of the local pitch-angle diffusion coefficient of the wave-particle interaction is derived as follows (see Eqs. (33)–(35) in Ref. [35]):

$$D_{\alpha\alpha} = \frac{\pi}{2}\frac{1}{\nu}\frac{\Omega_\sigma^2}{|\Omega_{\rm e}|}\frac{1}{(E+1)^2}\sum_j \frac{R(1-\frac{x\cos\alpha}{y\beta})^2|F(x,y)|}{\delta x|\beta\cos\alpha - F(x,y)|} \times \exp\left[-\left(\frac{x-x_{\rm m}}{\delta x}\right)^2\right], \quad (5)$$

$$\frac{D_{\alpha p}}{p} = \frac{\pi}{2}\frac{1}{\nu}\frac{\Omega_\sigma^2}{|\Omega_{\rm e}|}\frac{\sin\alpha}{\beta(E+1)^2}\sum_j \frac{R(\frac{x}{y})(1-\frac{x\cos\alpha}{y\beta})|F(x,y)|}{\delta x|\beta\cos\alpha - F(x,y)|} \times \exp\left[-\left(\frac{x-x_{\rm m}}{\delta x}\right)^2\right], \quad (6)$$

$$\frac{D_{pp}}{p^2} = \frac{\pi}{2}\frac{1}{\nu}\frac{\Omega_\sigma^2}{|\Omega_{\rm e}|}\frac{\sin^2\alpha}{\beta^2(E+1)^2}\sum_j \frac{R(\frac{x}{y})^2|F(x,y)|}{\delta x|\beta\cos\alpha - F(x,y)|} \times \exp\left[-\left(\frac{x-x_{\rm m}}{\delta x}\right)^2\right], \quad (7)$$

where E is the dimensionless particle kinetic energy given by $E = E_k/(m_\sigma c^2) = \gamma - 1$, $\beta = v/c = [E(E+2)]^{1/2}/(E+1)$, $R = |\delta B_s|^2/B_0^2$ is the ratio of the energy density of the turbulent magnetic field to that of the background field, and B_0 is the Earth's magnetic field. Further, $x_{\rm m} = \omega_{\rm m}/|\Omega_{\rm e}|$, $\delta x = \delta\omega/|\Omega_{\rm e}|$; and $j = 1, 2, \ldots, N$ is the root number satisfying the resonance condition. We have

$$\omega - v_\parallel k_\parallel = n\frac{|\Omega_\sigma|}{\gamma}. \quad (8)$$

Here we consider only cyclotron resonance with $n = \pm 1$. $F(x,y) = {\rm d}x/{\rm d}y$ ($x = \omega/|\Omega_{\rm e}|$, $y = ck_i/|\Omega_{\rm e}|$) is determined

from the dispersion equation of the electrons or protons as follows:

$$\left(\frac{ck}{\omega}\right)^2 = 1 - \frac{(1+\varepsilon)/\alpha^*}{(\omega/|\Omega_e| - 1)(\omega/|\Omega_e| + \varepsilon)}, \tag{9}$$

where

$$\alpha^* = \Omega_e^2/\omega_{pe}^2 \tag{10}$$

is an important cold-plasma parameter; ε is the rest mass ratio of an electron and proton; $|\Omega_e| = e|B|/(m_e c)$ denotes the electron gyrofrequency, and $\omega_{pe} = (4\pi N_0 e^2/m_e)^{1/2}$ is the plasma frequency, where N_0 denotes the particle number density in the ionosphere and is determined approximately by formula $N_0 = 50 \times (2/L)^4$ cm^{-3}, according to the observation from Van Allen probes (see supporting information of Ref. [27]).

The initial PSD distribution is approximately supposed to follow a kappa-type distribution function with the kappa index $\kappa = 6$:[36,37]

$$f(\alpha, p) = \left(1 + \frac{p^2}{\kappa\theta^2}\right)^{-(k+1)} \sin\alpha, \tag{11}$$

where α is the electron equatorial pitch angle, p is the electron momentum normalized by $m_e c$, m_e is the electron mass, c is the light speed, and θ is the effective thermal parameter scaled by the electron rest mass and is set as $\theta^2 = 0.15$. The PSD value is set to be zero with formula $f(\alpha \le \alpha_{LC}) = 0$; α_{LC} is the bounce loss cone determined by formula $\sin\alpha_L = L^{-3/2}(4 - 3/L)^{-1/4}$. The boundary condition of pitch angle is adopted to be $\frac{\partial f}{\partial \alpha}|_{\alpha=90^\circ} = 0$, and we set $f = f_0$ (0.01 MeV) = const at the lower boundary 0.01 MeV and $f = f_0$ (4 MeV) = const at the upper boundary 4 MeV. In this simulation the PSD is normalized and dimensionless.

3.2. Simulation results

According to the observed chorus waves by Van Allen probes at low L-shells, the bounce-averaged pitch angle diffusion coefficient $\langle D_{\alpha\alpha}\rangle$, momentum diffusion coefficient $\langle D_{pp}\rangle$, and their mixed term $\langle D_{\alpha p}\rangle$ in pitch angles $0 \sim 90^\circ$ for electrons at $L = 3$, 3.5 and 4, are calculated and present in Fig. 4.

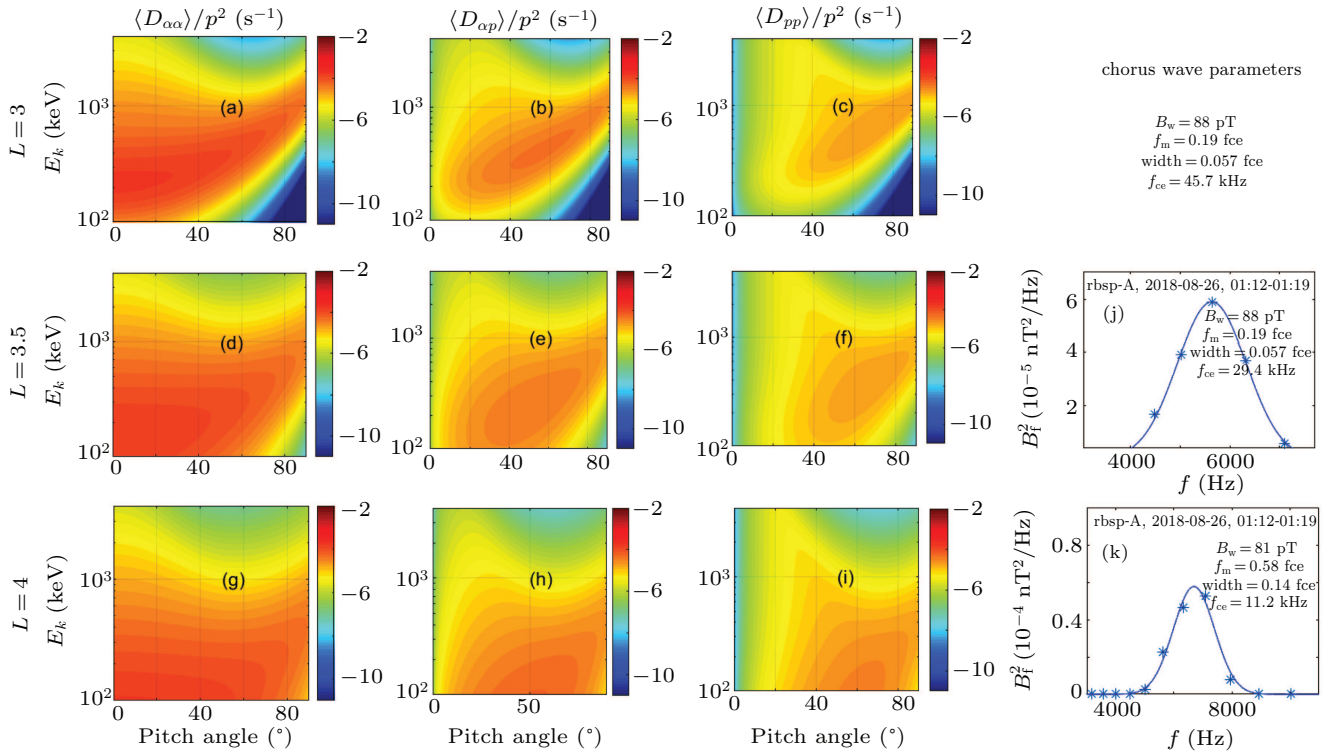


Fig. 4. (a)–(i) Bounce-averaged quasi-linear diffusion coefficients including pitch angle diffusion coefficient, momentum coefficient, and the cross term (in units of s^{-1}) for resonant interactions between chorus ad electrons, at $L = 3$, 3.5, 4, respectively. [(j), (k)] Wave parameters used in the calculations of diffusion coefficient from Van Allen probes observation.

The main feature of diffusion coefficients is that the momentum diffusion coefficients $\langle D_{pp}\rangle$ at low L-shells ($L \sim 3$ and 3.4) are very large, suggesting that those electrons at low L-shells are possibly easy to be accelerated to higher energies. What's more, the momentum diffusion coefficients for MeV electrons are relatively strong at low equatorial pitch angles 10°–40° nearby $L \sim 3$, indicative of an existence of stronger energy acceleration with respect to small equatorial pitch angles.

However, the key factor to determine the electron flux level comes from a competition between acceleration and loss due to chorus wave.[38] Therefore, we solve the 2-D Fokker–Planck equation and display the evolution processes of simulated electron fluxes j ($j = p^2 \times$ PSD, p is electron momentum) shown in Fig. 5 corresponding to $L = 3.5$, at initial time, 1 h, 5 h, 10 h,

15 h and 24 h, respectively. We can find that after 24 h the flux evolution tends to be a stable level, suggesting that the chorus acceleration effect mainly takes place in about tens of hours. For MeV electrons in pitch angle 10°–50°, the corresponding fluxes are enhanced significantly, which is induced by chorus acceleration.

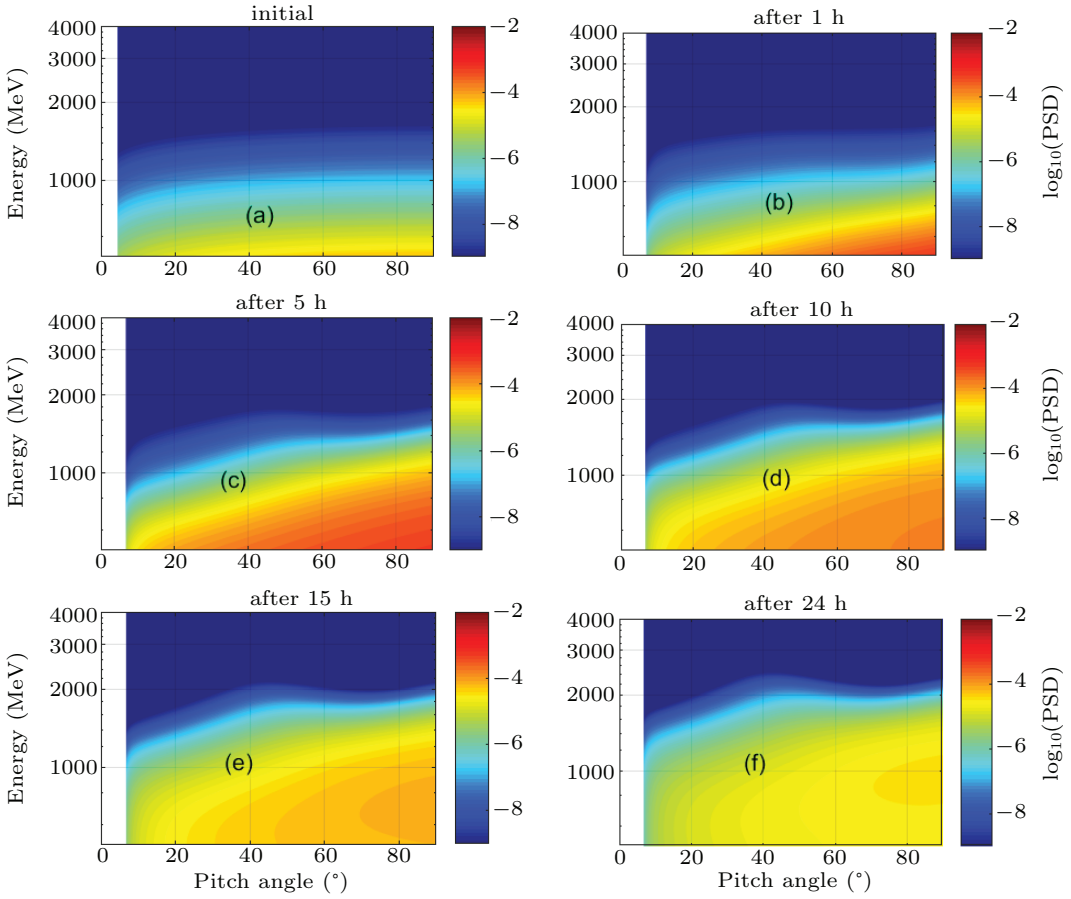


Fig. 5. The electron flux evolution during 2D numerical simulation of the interaction of chorus and electrons at $L = 3.5$.

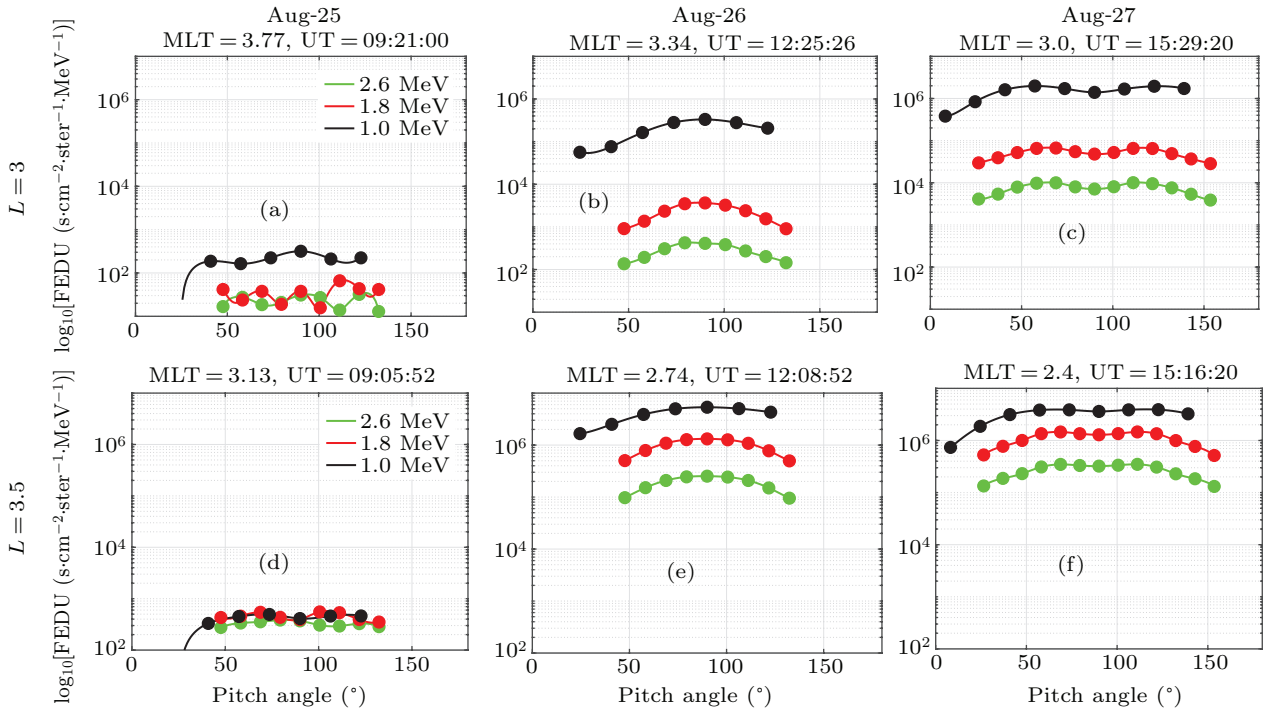


Fig. 6. Evolution of fluxes and pitch angles distribution of electrons (1 MeV, 1.8 MeV and 2.6 MeV) observed from MagEIS and REPT detectors onboard Van Allen probes before and during storm time on 25, 26 and 27 August 2018: (a)–(c) at $L = 3$, (d)–(f) at $L = 3.5$.

The aforementioned butterfly pitch angle distribution of MeV electrons, observed by Van Allen probes on August 27 during the recovery phase of storm, has been presented in Figs. 6(c) and 6(f). The enhanced MeV electrons correspond to the equatorial pitch angle range of 10°–60° based on ZH-1 observation. We present flux and pitch angle distributions for electrons at 1 MeV, 1.8 MeV and 2.6 MeV in Fig. 6 corresponding to $L = 3$ and 3.4, respectively, on 25, 26 and 27 August 2018. These plots display the whole evolution process of electron fluxes and pitch angles before and after storms at low L-shells. On August 25–27, the fluxes of MeV electrons are accelerated significantly by around 2 orders of magnitude.

In order to compare the numerical simulation results with observations, we extract the fluxes and pitch angle distributions for electrons at 1 MeV, 1.8 MeV and 2.6 MeV from simulation results shown in Fig. 7, corresponding to initial and 24-h flux distributions. It is found that the significant accelerations and butterfly pitch angle distributions are caused by chorus heating mechanism after one day interval at low L-shells. Here we set the flux value to be a suitable level in order to intuitively compare with observations for the sake of convenience. In the simulation results, the fluxes at small pitch angles are enhanced by about two orders of magnitude, more significantly for MeV electrons. Therefore, our simulation results are approximately in agreement with the observations and further confirm that the chorus waves can play an important role in accelerating relativistic electrons even in extremely low L-shell regions during major storm occurrence.

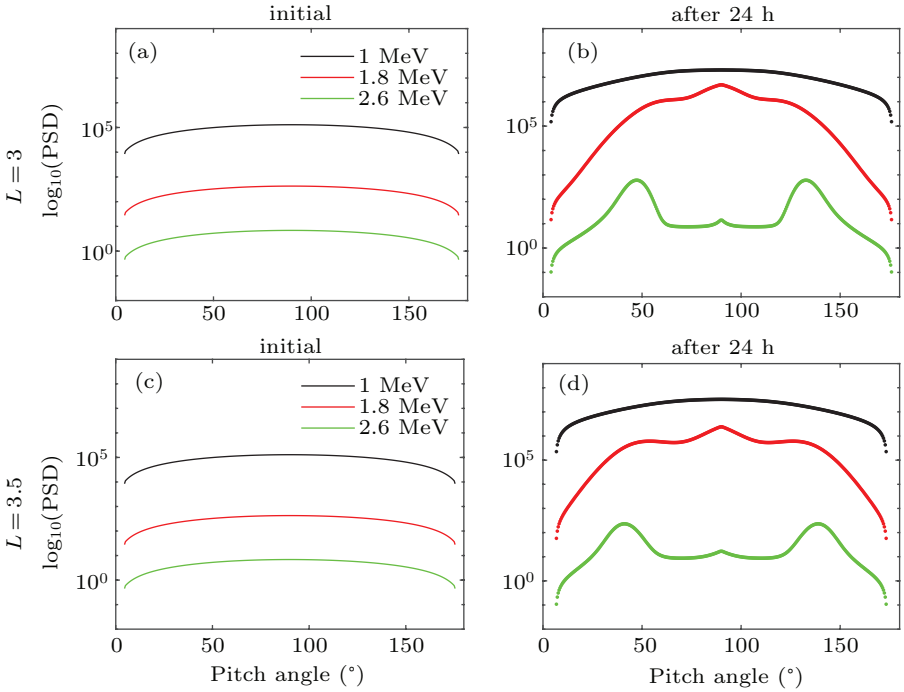


Fig. 7. Simulation results of electron PSD evolutions (1 MeV, 1.8 MeV and 2.6 MeV) for chorus and electron interaction at initial time (left panels) and after 24 h (right panels): [(a), (b)] at $L = 3$, [(c), (d)] at $L = 3.5$.

4. Conclusion and discussion

First of all, we introduce the event of relativistic electron acceleration in extremely low L-shell regions induced by interaction with chorus waves observed during 2018 major geomagnetic storm by Van Allen probes and the ZH-1 satellite. As the main content of this paper, we perform 2-D numerical simulation by solving the Fokker–Planck equation based on bounce-averaged diffusion rates, following the method of HFD solution.[22] In term of the simulation results, we conclude the following results and give some discussions.

Based on bounce-averaged diffusion coefficients using a fitting Gaussian distribution of the wave spectrum, the 0.1–3 MeV electron fluxes are simulated at low L-shells ($L = 3$, 3.5 and 4) for 24 h and the flux evolution processes are present. We adopted a plasma density according to observation of Van Allen probes with $N_0 \approx 10$ at $L = 3$, which is different from the value used in Ref. [27]. The electron flux level is determined by a competition between acceleration and loss due to wave-particle interaction.

In final simulation results, the electrons are most pronounced around small pitch angles 10°–50° due to the dominant momentum and cross diffusion processes. Thus, the pitch angle distribution changes from a normal type into a potential butterfly type, which is consistent with observations of Van Allen probes and the ZH-1 satellite.

We can also find that there is much disagreement between observations and numerical simulation results, such as the pitch angle ranges of the most enhanced flux, the not completely consistent flux evolution level and the failure of butterfly pitch angle distribution formation of 1 MeV electrons.

These disagreements can be caused by many kinds of reasons. Van Allen probes observation we show in this paper is just from data at nightside, in fact the chorus occurs not only at nightside, but also lasting for a long time of two days in a considerable wide spatial region. Unfortunately, the precise quantitative simulation calculation is much too difficult and sometimes it is impossible due to the complicated spatial environment and observation limitation. Therefore, in this paper the disagreement may exist inevitably between the observations and simulations.

During geomagnetic storms, sometimes the electron acceleration may be simultaneously caused by chorus and magnetosonic waves (MS).[10] We also carefully investigated the two kinds of waves precisely and found that the MS waves mainly exist in $L <= 3$ (see Fig. 2). According to the diffusion coefficient calculation, MS waves mostly induce electron acceleration in larger equatorial pitch angles ($> 50^{\circ}$), which is supported by our satellite data observation (not shown) and the diffusion coefficients.[10] Thus, in term of the acceleration in small equatorial pitch angles and in $L >= 3$ area, the chorus driving is the main cause of electron acceleration.

In summary, we have reported the chorus acceleration of relativistic electrons at extremely low L-shell region during storm based on joint observation of Van Allen probes and the ZH-1 satellite, and now we have further confirmed this physics phenomenon by numerical simulation of a quasi-linear diffusion equation in wave-particle interaction theory. The simulation results also support the above viewpoint that the chorus waves can cause potential butterfly pitch angle distributions during major storm when the plasmapause is strongly suppressed inward. It is very meaningful and helpful to deeply understand the electron acceleration process in radiation belt physics.

References

[1] Lyons L R and Thorne R M 1973 *J. Geophys. Res.* **78** 2142

[2] Meredith N P, Horne R B, Glauert S A, Baker D N, Kanekal S G and Albert J M 2009 *J. Geophys. Res.***114** A03222

[3] Ni B B, Bortnik J, Thorne R M, Ma Q and Chen L 2013 *J. Geophys. Res.* **118** 7740

[4] Blake J B, Kolasinski W A, Fillius R W and Mullen E G 1992 *Geophys. Res. Lett.* **19** 821

[5] Rodger C J, Clilverd M A, Green J C and Lam M M 2010 *J. Geophys. Res.***115** A04202

[6] Meredith N P, Horne R B, Lam M M, Denton M H, Borovsky J E and Green J C 2011 *J. Geophys. Res.***116** A05223

[7] Kavanagh A J, Cobbett N, and Kirsch P 2018 *J. Geophys. Res.* **123** 7999

[8] Xiao F, Su Z, Zheng H and Wang S 2010 *J. Geophys. Res.***115** A05216

[9] Li W, Mourenas D, Artemyev A V, Bortnik J, Thorne R M, Kletzing C A, Kurth W S, Hospodarsky G B, Reeves G D, Funsten H O and Spence H E 2016 *Geophys. Res. Lett.***43** 8867

[10] Xiao F L, Chang Y, Su Z P, Zhou Q H, He Z G, He Y H, Baker D N, Spence H E, Funsten H O, Blake J B 2015 *Nat. Commun.* **6** 8590

[11] Jin Y Y, Yang C, He Y H, Liu S, Zhou Q H and Xiao F L 2018 *Sci. China: Tech. Sci.* **61** 212

[12] Sheeley B W, Moldwin M B, Rassoul H K, and Anderson R R 2001 *J. Geophys. Res.* **106** 25631

[13] LeDocq M J, Gurnett D A and Hospodarsky G B 1999 *Geophys. Res. Lett.* **25** 4063

[14] Santolík O, Parrot M and Lefeuvre F2003 *Radio Sci.* **38** 1010

[15] Li W, Ni B, Thorne R M, Bortnik J, Green J C, Kletzing C A, Kurth W S and Hospodarsky G B 2013 *Geophys. Res. Lett.* **40** 4526

[16] Tao X, Zonca F and Chen L 2017 *Geophys. Res. Lett.* **44** 3441

[17] Thorne R M 2013 *Nature* **504** 411

[18] Bortnik J, Inan U S and Bell T F 2006 *J. Geophys. Res.* **111** A02205

[19] Chen Y, Reeves G D and Friedel R H W 2007 *Nat. Phys.* **3** 614

[20] Liu S, Xiao F L, Yang C, He Y H, Zhou Q H, Kletzing C A, Kurth W S, Hospodarsky G B, Spence H E, Reeves G D, Funsten H O, Blake J B, Baker D N, and Wygant J R 2015 *J. Geophys. Res.* **120** 938

[21] Liu S, Yan Q, Yang C, Zhou Q, He Z, He Y 2018 *Geophys. Res. Lett.* **45** 1262

[22] Xiao F, Su Z, Zheng H, and Wang S 2009 *J. Geophys. Res.* **114** A03201

[23] Xiao F L, Yang C, He Z G, Su Z P, Zhou Q H, He Y H, Kletzing C A, Kurth W S, Hospodarsky G B, Spence H E, Reeves G D, Funsten H O, Blake J B, Baker D N and Wygant J R 2014 *J. Geophys. Res.* **119** 3325

[24] Su Z, Zheng H and Wang S 2009 *J. Geophys. Res.* **114** A08202

[25] Zeren Z, Cao J, Liu W, Fu H, Yang J, Zhang X and Shen X 2013 *Geophys. Res. Lett.* **40** 5827

[26] Fu H S 2014 *J. Geophys. Res.* **119** 9089

[27] Zhang Z, Chen L, Liu S, Xiong Y, Li X, Wang Y 2020 *Geophys. Res. Lett.* **47** e2019GL086226

[28] Shen X H, Zhang X M, Yuan S G, Wang L W, Cao J B and Huang J P 2018 *Sci. China: Tech. Sci.* **61** 634

[29] Li X Q, Xu Y B, An Z H, Liang X H, Wang P, Zhao X Y *et al.* 2019 *Radiat. Detect. Technol. Methods* **3** 22

[30] Mauk B H, Fox N J, Kanekal S G, Kessel R L, Sibeck D G and Ukhorskiy A 2013 *Space Sci. Rev.* **179** 3

[31] Baker D N, Kanekal S, Hoxie V, Batiste S, Bolton M, Li X *et al.*2012 *Space Sci. Rev.* **179** 337

[32] Kletzing C A, Kurth W S, Acuna M, MacDowall R J, Torbert R B, Averkamp T and Tyler J 2013 *Space Sci. Rev.* **179** 127

[33] Kim H J and Chan A A 1997 *J. Geophys. Res.* **102** 22107

[34] Li X L, Barker A B, Baker D N, Tu W C, Sarris T E, Selesnick R S Friedel R and Shen C 2009 *Space Weather* **7** S02004

[35] Summers D 2005 *J. Geophys. Res.* **110** A08213

[36] Xiao F, Shen C, Wang Y, Zheng H and Wang S 2008 *J. Geophys. Res.* **113** A05203

[37] Ma Q, Li W, Thorne R M, Bortnik J, Kletzing C A, Kurth W S and Hospodarsky G B 2016 *J. Geophys. Res.* **121** 274

[38] Bortnik J and Thorne R M 2007 *J. Atmosperic Solar-Terrestrial Phys.* **69** 378